
[View Journal Online](#)
[View Article Online](#)

A density functional study of the coronene-pyrrole system in relation to its possible application as NO₂ and NH₃ sensors

Cintha Susana Olmedo-Martínez ¹, Jesús Moisés Hernández-Duarte ²,
 Roberto Mejía-Olvera ^{1,3}, Sandy-María Pacheco-Ortín ¹, and Esther Agacino-Valdés ^{1,4,*}

¹ Departamento de Química, Facultad de Estudios Superiores Cuautitlán, Universidad Nacional Autónoma de México, Cuautitlán Izcalli, CP 54740, Estado de México, México

² Centro de Tecnologías en Cómputo y Comunicación, Facultad de Estudios Superiores Cuautitlán, Universidad Nacional Autónoma de México, Cuautitlán Izcalli, CP 54740, Estado de México, México

³ Departamento de Ingeniería Industrial, Tecnológico de Estudios Superiores de Cuautitlán Izcalli, Cuautitlán Izcalli, CP 54748, Estado de México, México

⁴ Centro de Investigaciones Teóricas, Facultad de Estudios Superiores Cuautitlán, Universidad Nacional Autónoma de México, Cuautitlán Izcalli, CP 54740, Estado de México, México

* Corresponding author at: Departamento de Química, Facultad de Estudios Superiores Cuautitlán, Universidad Nacional Autónoma de México, Cuautitlán Izcalli, CP 54740, Estado de México, México.

e-mail: [eagacino@unam.mx](mailto: eagacino@unam.mx) (E. Agacino-Valdés).

RESEARCH ARTICLE



doi 10.5155/eurjchem.13.4.371-380.2316

Received: 30 July 2022

Received in revised form: 05 September 2022

Accepted: 09 September 2022

Published online: 31 December 2022

Printed: 31 December 2022

KEYWORDS

Adsorption
 NO₂-adsorption
 NH₃-adsorption
 Pyrrole-graphene interaction
 Coronene-pyrrole interaction
 Density functional calculations

ABSTRACT

According to recent research on the application of graphene materials as sensors and particularly polypyrrole-graphene materials, which are especially promising, the functionalization of graphene with a pyrrole molecule might be considered a viable alternative as a NO₂ and NH₃ sensor. In this way, a graphene sheet simulated as a coronene molecule was used in order to test whether this kind of functionalization could be useful for detecting the NO₂ and NH₃ toxic gases with a relatively high sensitivity. NO₂ was studied as an example of an electron acceptor molecule, and NH₃ as an electron donor molecule. Both molecules were adsorbed on two different regions of the functionalized adsorbent, and the energy ranges found for adsorption were reported and compared with those of the pristine graphene. The results indicated that in the coronene-pyrrole system, pyrrole tends to lie almost parallel to the coronene sheet in a π - π stacking interaction between the two conjugated systems, being the closest distances of 3.0 and 3.2 Å. The use of Δ ($\Delta_{\text{HOMO-LUMO}}$) as a descriptor confirmed that the coronene-pyrrole system is a good option as a NO₂- and NH₃-sensor; therefore, it might be an easy and suitable descriptor for characterizing the performance of a sensor; all calculations were made using a Density Functional formalism, through a functional M06-2X in combination with the 6-31G(d,p) basis set.

Cite this: *Eur. J. Chem.* 2022, 13(4), 371-380

Journal website: www.eurjchem.com

1. Introduction

Since graphene was discovered in 2004 [1], the interest for this material has grown extensively in the last decade due to its unique mechanical and electronic properties and by a high charge carriers' mobility [2-5]. Particularly, the graphene ability for adsorbing gas molecules has led to using it as a chemical sensor. As it is known, the operational principle of a graphene chemical sensor is based on changes in their electrical conductivity, because of gas molecules adsorbed on their surface and acting as electron donors or electron acceptors; one of the first reports about gas molecules adsorbed on pristine graphene was published in 2007 by Schedin, *et al.* [6], which showed that a micrometer-size sensor could detect individual gas molecule and confirmed experimentally the adsorption of NO₂, NH₃, H₂O and CO. Besides, they explained that adsorbed molecules could change the local carrier charges concentration in graphene and therefore, its resistance. Finally, they also

concluded that this material seems promising as a gas chemical detector. Since then, many investigations have been developed that focus on exploring the capacity of modified graphene materials to detect individual gases with relatively high sensitivity [7]. Various authors have reported recent progress in the field of graphene gas sensors with emphasis on the use of modified or functionalized graphene materials [8-10]. In this way, the so-called graphene-based nanomaterials (GBN) have recently been applied in a broad range of science and technology fields and are promising devices in nanomedicine, biosensors, energy storage, and power generation, taking advantage of their unique electronic structure and possibilities to be modified [11]. For instance, the graphene surface has been functionalized with organic molecules such as dialcohols, diamines, and dithiols [12]. Particularly, Yu *et al.* performed a DFT study of the non-covalent interaction between pristine graphene and some aromatic molecules including thiophene, benzene, and pyridine. In this study, the aromatic rings of this

molecules were placed on the top of the graphene surface at the height of 3.5 Å in both parallel and vertical orientation. The results demonstrated that the non-covalent interactions between the aromatic molecules and the graphene surface originate mainly from the π - π stacking effect between the two conjugated systems [13].

The structural and electronic properties of the graphene-molecule adsorption complex are strongly dependent on the graphene structure and the end configuration of the adsorption complex. In this way, it has already been shown that perfect graphene predicts relatively low adsorption energies compared to the essential requirement for gas detection by sensors [14]. Therefore, the sensitivity of graphene-based chemical gas sensors could be drastically improved by introducing appropriate functionalization or structural defects. In addition, the functionalization of pristine graphene sheets with organic molecules containing specific functional groups has also been developed [15]. Particularly, functionalized graphene sensors showed improved performance in comparison with those without functionalization in terms of selectivity, sensitivity, and limit of detection, which has contributed to improve the commercialization and technological developing of these devices [16]. Promising advances in increased selectivity have been achieved for some gases, including NH_3 , NO_2 , and a variety of volatile organic compounds (VOCs). Tang *et al.* [17] have summarized the recent development of functionalized graphene sensors for the detection of ammonia (NH_3) at room temperature, considering metallic nanoparticles, metal oxides, organic molecules, and conducting polymers. They have highlighted that functionalized based graphene NH_3 -sensors will have a bright perspective due to the advantages of high sensitivity, fast response, great selectivity, low power consumption, cost-effectiveness, and operation in real-life conditions; these sensors are essential for industrial emission control, environment conservation, and human safety.

An interesting variety of new graphene materials are conductor polymers (CPs) [18] like polythiophene, polyaniline (PANI), poly-(phenylene vinylene) and polypyrrole (PPy); this CPs materials are being used as chemical and biochemical sensors due to its high sensitivities, fast response times, and room temperature operation. Particularly, in this CPs group, PPy has been widely used mainly because of its good electrical conductivity, environmental stability, good biocompatibility, as well as its facile synthesis and versatility compared to the other CPs [19]. Another well-known CPs are polyaniline nanofibers (PANI), which are adsorbed on graphene [20,21] and nanocomposites [22], which have been used as hydrogen gas sensors with good performance. On the other hand, Liu *et al.* [23] have reported the synthesis, transport studies, and NO_2 and NH_3 sensing applications in individual single walled carbon nanotubes functionalized with polypyrrole nanocables (SWCNT/PPy); they have confirmed that this material enhances conductance when it is exposed to an oxidizing gas such as NO_2 , and reduced it when it was exposed to a reducing gas such as NH_3 , in concordance with the electron acceptor and electron donor characteristics of these species.

Using DFT studies, Leenaerts *et al.* [24] showed that the CO , NH_3 , NO_2 , H_2O , and NO molecules are physically adsorbed on pristine graphene. Likewise, Bonfanti *et al.* [25] computed at MP2 level the hydrogen physisorption energy (39.7 meV) in excellent agreement with the experiment, using a hydrogen-coronene model; other studies confirmed that NO_2 acted as an electron-acceptor while NH_3 performed as an electron-donor, in agreement with the experimental findings of Schedin *et al.* [6]. Furthermore, combined DFT calculations together with in situ-infrared spectroscopy experiments of NH_3 adsorbed on reduced graphene oxide (RGO), have revealed that NH_3 adsorption occurred by a physisorption process and different fragment species were identified [26]. Moreover, Jang *et al.* [27] obtained experimentally a NH_3 gas sensor based on the PPy/graphitic

material nanocomposites (GO and RGO), and the Raman spectra of PPy/RGO nanocomposites demonstrated a π - π interaction at the interface PPy/RGO of this nanocomposite as well as a very favorable response in detecting NH_3 gas. They observed and attributed these outcomes to the effective charge transfer at the interface between PPy and NH_3 , and the interfacial interaction between PPy and RGO graphene sheet.

Taking all these evidence and research into account, there are some aspects that could be explained throughout a theoretical study. For example, the relation between the change of conductance in the graphene material when exposed to NO_2 and NH_3 , or why in the Jang *et al.* studies of PPy/RGO nanocomposite, they related the favorable response in detecting NH_3 to an effective charge transfer at the interface PPy/ NH_3 and PPy/RGO. To our knowledge, no theoretical studies have been performed to clarify NO_2 and NH_3 interactions with pyrrole functionalized graphene. Therefore, in our work, graphene functionalization with a pyrrole monomer was carried out, using a coronene molecule as a graphene finite model; after these calculations, the formation of NO_2 -pyrrole/coronene and NH_3 -pyrrole/coronene adsorption complexes was considered to evaluate the possibilities of both systems to perform themselves as gas sensors for these two toxic gases.

2. Experimental

2.1. Software and theory

The calculations were carried out using the Gaussian09 package [28] and applying a density functional formalism through the correlation and exchange functional M06-2X [29] in combination with the 6-31G(d,p) basis set. This DFT-functional has been recommended for applications in conjugated polyenes and noncovalent interactions [30] because it performs strikingly well in this kind of molecular system.

2.2. Methodology

The modeled structures were fully optimized, and their corresponding frequency calculations were carried out, confirming that a minimum energy was obtained in all geometries. In this study, a coronene ($\text{C}_{24}\text{H}_{12}$) molecule was chosen as a graphene sheet molecular model, which has been a strategy used in many previous works [31-38], having proven that coronene-based model can be considered a suitable model for studying this kind of process. As can be seen in Figure 1, the presence of hydrogen atoms is essential because they saturate the dangling bonds of edge carbons; this figure shows a pristine coronene model simulating a pristine-graphene sheet.

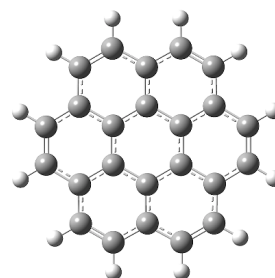


Figure 1. Optimized geometry of pristine coronene.

The adsorption energies (E_{ads}) of pyrrole molecule (Py) over pristine coronene sheet (C) to form the coronene-pyrrole adsorption complex were obtained from Equation (1); likewise, the adsorption energies of NH_3 and NO_2 molecules (M_{ads}) over pristine coronene sheet (C) and coronene-pyrrole complex (Py-C) were obtained from Equations (2) and (3).

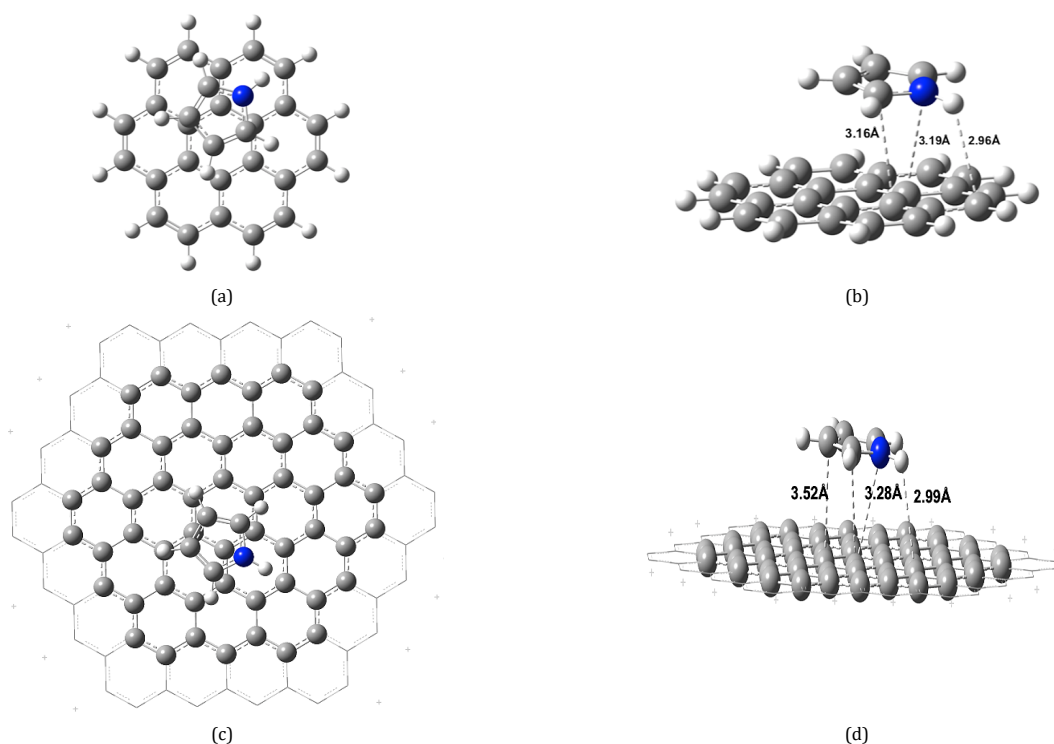


Figure 2. Optimized geometry of the coronene-pyrrole adsorbent complex in a top (a) and side (b) view and polycircumcoronene-pyrrole adsorption complex in a top (c) and side (d) views.

Notice that a positive value of the adsorption energy indicates that the adsorption process occurred favorably. These equations are shown below.

$$E_{ads} = E(Py) + E(C) - E(Py - C) \quad (1)$$

$$E_{ads} = E(M_{ads}) + E(C) - E(M_{ads} - C) \quad (2)$$

$$E_{ads} = E(M_{ads}) + E(Py - C) - E(M_{ads} - Py - C) \quad (3)$$

To study the coronene-pyrrole system, pyrrole was placed near the sheet of coronene in a parallel and perpendicular position (at 3.8, 3.4, 3.0, 2.6, 2.2 and 1.8 Å). Subsequently, the pyrrole-coronene geometry with the best adsorption energy was used to study the NH₃ and NO₂ adsorptions for validating the use of the coronene (C₂₄H₁₂) molecule as a graphene sheet-like molecular model.

For evaluating if the size of the coronene sheet (C₂₄H₁₂) would be suitable to describe pyrrole adsorption, and the edge effects would not influence on the optimized geometry, the ONIOM methodology [39,40] was implemented for modeling a larger system, the polycircumcoronene sheet of 96 carbon atoms (C₉₆H₂₄). This methodology provides a strategy for using accurate (an expensive) quantum mechanics methods (QM) on only that part of the molecule or cluster that comprises the chemically active region. Therefore, the complete molecular system is partitioned into two or three defined subunits or layers. For a two-layer partition, in one of the layers, a QM method is used, which represents a high level of calculation; the other layer represents the low-level of theory and can be used as methods of molecular mechanics (MM), semiempirical (SE) or a simpler QM method.

In our large molecular system, a QM/SE ONIOM model was used. The high-level of theory layer was formed by the pyrrole molecule and the circumcoronene sheet of 54 carbon atoms; this layer was treated at the QM-DFT level, using the combination of M06-2X exchange and correlation functional with the

basis set 6-31G(d,p). On the other hand, the outer low-level of theory layer (C₄₂H₂₄) was treated at the semiempirical (SE) level using the PM3 method. Figure 2 (c and d) presents the optimized geometry of the polycircumcoronene-pyrrole adsorption complex (C₉₆H₂₄) considering the ONIOM model described above, in top and side views. Notice that the high-level layer of theory is represented by balls and sticks, and the lower level by tubes.

Considering that the NO₂ molecule is an electron acceptor and NH₃ is an electron donor, these molecules were approached to sites with high and low electron density, respectively, which were identified by Hirshfeld charge analysis. The approaching sites included an atom, a bond line, and a center of a hexagon located in two different regions of the adsorbent complex: the free site coronene sheet and the pyrrolic ring. In each configuration, the adsorbate molecules were oriented in a parallel and perpendicular position to the coronene sheet at 3.4, 3.0, 2.6, 2.2, and 1.8 Å of distance. For the perpendicular orientation, two possibilities were tested for each gas molecule, with two kinds of atoms pointing towards the coronene, nitrogen and oxygen atoms for NO₂ and nitrogen and hydrogen atoms for NH₃. The different configurations considered allowed us to identify the most probable distance between the adsorbent and adsorbate molecules and its most effective orientation. In addition, the corresponding adsorption energy has led us to decide whether the adsorption is physical or chemical. Finally, to know if the presence of NH₃ or NO₂ yielded changes in the electronic properties of the adsorbent, the difference between the gap HOMO-LUMO [24] before and after a gas molecule was adsorbed on the coronene-pyrrole adsorbent complex called Δ ($\Delta_{\text{HOMO-LUMO}}$), was calculated. Since a physisorption processes involving weak interactions is produced, the adsorption energy and the Δ ($\Delta_{\text{HOMO-LUMO}}$) are expressed in meV [24,25]; in this way, the calculation could require until four decimals. Likewise, the Hirshfeld charge transfers are indicated in 10⁻²e order [24].

Table 1. Adsorption energies (E_{ads}) in meV; the HOMO and LUMO energies, the difference ($\Delta E_{\text{HOMO-LUMO}}$) between the pristine coronene and the coronene-pyrrole adsorbent complex and the magnitude of Δ ($\Delta_{\text{HOMO-LUMO}}$) in eV.

Compound	E_{ads}	E_{HOMO}	E_{LUMO}	$\Delta E_{\text{HOMO-LUMO}}$	Δ ($\Delta_{\text{HOMO-LUMO}}$)
Pristine coronene	-	-6.6203	-0.7181	5.9022	-
Coronene-pyrrole complex	344.9	-6.3498	-0.6623	5.6875	-0.2147

**Figure 3.** HOMO (a) and LUMO (b) frontier orbitals of the coronene-pyrrole adsorbent complex.

The parameter Δ ($\Delta_{\text{HOMO-LUMO}}$), can be considered a descriptor associated with the potential sensor performance of a material. It is known that a fundamental principle of sensor operation is based on the change of resistance of the adsorbent matrix. In this case, the graphene sheet is used when the gas molecules are adsorbed on the latter.

3. Results and discussion

3.1. Coronene-pyrrole vs. polycircumcoronene-pyrrole adsorbent complexes

About the interaction between coronene and pyrrole molecules, the results indicated that pyrrole tends to locate itself almost parallel to the sheet of coronene with a slight deviation of approximately 5° and a range of 3.0-3.4 Å of distance; in this way, a noncovalent π - π stacking interaction was found, as it can be seen in Figure 2a and 2b, with an adsorption energy of 344.9 meV (Table 1). This outcome is consistent with the experimental finding of Jang *et al.* [27] in PPy/RGO nanocomposite materials and other studies using aromatic molecules [41]. Figure 2b shows the closest distances between pyrrole and coronene molecule which correspond to 2.96 (H-C), 3.16 (C-C), and 3.19 Å (N-C). On the other hand, the longest distance was 3.46 Å. The distances indicated above (Figure 2) confirm the presence of Van der Waals force in the coronene-pyrrole interaction.

The optimized geometry of the polycircumcoronene-pyrrole adsorption complex showed in Figure 2c and 2d allows to conclude that the arrangement of the pyrrole molecule was very similar to the coronene sheet. In the ONIOM model, the pyrrole molecule tends to locate itself almost parallel to the sheet of polycircumcoronene, although in somewhat greater angle (12°). Similarly, the closest distances between the pyrrole molecule and polycircumcoronene corresponded to 2.99 (H-C), 3.52 (C-C), and 3.28 Å (N-C). On the other hand, the longest distance was 3.52 Å.

The non-significant differences found in both models allow us to assert that, as other authors have stated, the coronene molecule could be a good graphene sheet molecular model for studying the adsorption process when an adsorbate molecule, such as pyrrole, has smaller dimensions than the coronene's hexagons. Therefore, the subsequent adsorption studies were conducted using the coronene ($\text{C}_{24}\text{H}_{12}$) molecule as an adsorbent.

3.2. Electronic properties of the coronene-pyrrole adsorbent complex

The calculated Hirshfeld charges showed that the carbon and nitrogen atoms of pyrrole, exhibited negative charge values

(-0.03e, -0.03e and -0.10e), and consequently, the coronene's carbon atoms located at central hexagon and close to pyrrole, were deactivated in charge; in this way, a slight charge transferred from coronene to pyrrole via the nearest atoms of both molecules; however, coronene kept the negative charge in the carbon atoms external to the central hexagon. In general, the coronene-pyrrole complex has available activated and deactivated sites which could favor the NO_2 and NH_3 adsorptions.

Table 1 shows the HOMO and LUMO energies of pristine coronene and the coronene-pyrrole complex. The respective HOMO-LUMO gaps and the magnitude of the change produced by the presence of pyrrole. The HOMO-LUMO ($\Delta_{\text{HOMO-LUMO}}$) gap in this π - π complex was of 5.69 eV, smaller than the pristine coronene gap (5.90 eV).

The variation of the gap, that is, Δ ($\Delta_{\text{HOMO-LUMO}}$) was 214.7 meV. These magnitudes indicate that, even though the interaction energy coronene-pyrrole is weak, the electron-acceptor character of pyrrole has produced a slight change in the HOMO-LUMO gap in relation to the pristine coronene molecule. In this way, both orbitals, HOMO and LUMO, increased their respective energies, but the rise in the HOMO orbital (270.5 meV) was larger than LUMO (55.8 meV); therefore, because of this functionalization, a narrowest gap HOMO-LUMO occurred. The reason for the larger change in the HOMO orbital can be found in Figure 3, where both frontier orbital maps, HOMO and LUMO, are presented. Notice the π character of both frontier orbitals and the presence in the HOMO map of the whole coronene-pyrrole complex; the π -molecular orbitals are extended not only over the coronene sheet but also over the pyrrole molecule. As a result of the interaction and the effective charge transfer produced between these two molecules, the HOMO domain was increased.

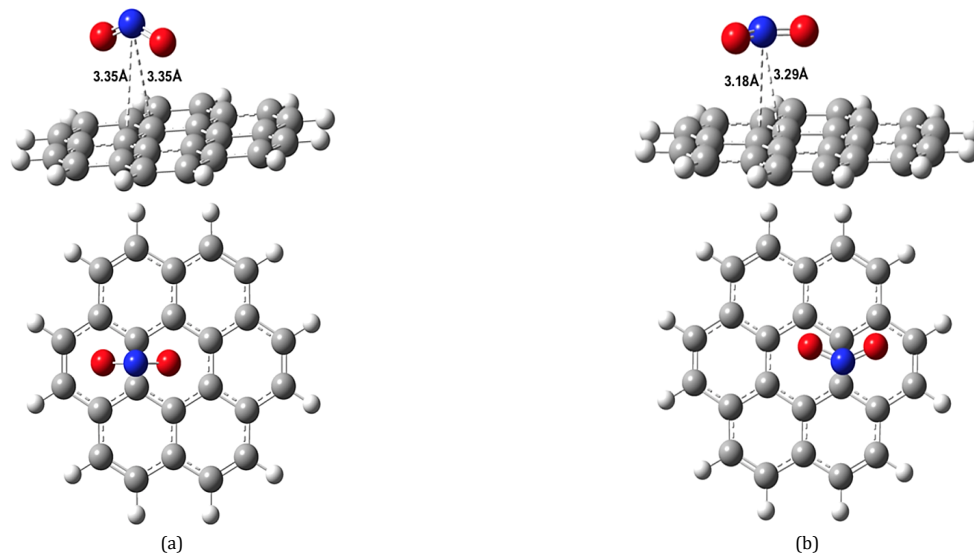
3.3. NO_2 adsorption on pristine coronene

Firstly, the interaction between NO_2 and pristine coronene was studied; the adsorption energy range obtained was around 175-207 meV (Table 2). Figure 4 shows the most favorable positions. Figure 4a shows NO_2 in interaction with the coronene molecule through oxygen atoms in the top (bottom of the figure) and side (top of the figure) views; in this final geometry, nitrogen has stayed over a C-C bond and each oxygen over the center of a ring; when one of the rings is the central one, the adsorption energy is larger ($E_{\text{ads}} = 207.12$ meV) than in the case in which the central ring is not participating ($E_{\text{ads}} = 193.28$ meV). The N-C distance is at 3.35 Å and the O-C distance is about 3.0-3.2 Å.

In Figure 4b, NO_2 interacts with the coronene molecule through its nitrogen atom, although, as well as in Figure 4a, the

Table 2. Adsorption energy in meV; $\Delta_{\text{HOMO-LUMO}}$ in eV and Δ ($\Delta_{\text{HOMO-LUMO}}$) values in meV for NO_2 adsorption.

Adsorption complex	E_{ads}	$\Delta_{\text{HOMO-LUMO}}$	Δ ($\Delta_{\text{HOMO-LUMO}}$)
NO_2 -Coronene	175-207	5.2303	-671.9 *
NO_2 -pyrrole-coronene (Coronene free sites)	240-279	4.8186	-868.9 **
NO_2 -pyrrole-coronene (On pyrrole)	181-224	5.1111	-576.4 **

* Obtained in respect of pristine coronene ($\Delta_{\text{HOMO-LUMO}} = 5.9022$ eV).** Obtained in respect of coronene-pyrrole ($\Delta_{\text{HOMO-LUMO}} = 5.6875$ eV).**Figure 4.** The two most representative optimized geometry of NO_2 adsorbed on pristine coronene molecule (a, b).**Figure 5.** The most stable optimized geometry for NO_2 adsorption on the coronene-pyrrole system considering the NO_2 -entry into the free sites of coronene (a) and over the pyrrole ring (b).

oxygen atoms have also kept over the two coronene hexagons, almost pointing to the coronene carbon atoms. The final geometry indicates that nitrogen has remained on the bridge at 3.18 and 3.29 Å from the two closest carbon atoms and the O-C distances were slightly larger, in the range of 3.23-3.28 Å (Figure 3a); in this case, the NO_2 molecule aligned parallel in relation to the coronene sheet. In Figure 3a, when the central hexagon is participating in the interaction with the oxygens, the adsorption energy is larger ($E_{\text{ads}} = 200.10$ meV) than the geometry in which the central ring was not involved ($E_{\text{ads}} = 179.73$ meV).

Finally, another configuration could be found, when the NO_2 molecule was located in the center of the central hexagon with nitrogen near the coronene sheet and oxygen atoms pointing upward, the adsorption energy was the smallest obtained ($E_{\text{ads}} = 175.01$ meV).

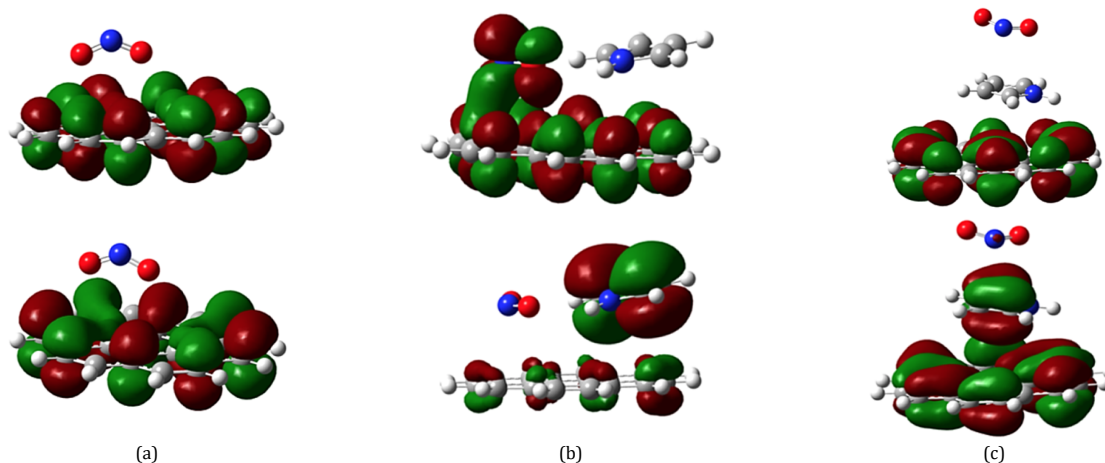
3.4. NO_2 adsorption on the coronene-pyrrole adsorbent system

Figure 5a shows a configuration in which NO_2 is placed, over the free sites of coronene; notice that the final geometry is placed in parallel position with respect to the coronene plane; each oxygen atom of NO_2 , interacts with one hydrogen of the pyrrolic ring in a clear hydrogen bond. This configuration

showed the highest adsorption energy ($E_{\text{ads}} = 279.39$ meV) of this adsorbent complex, but also higher than pristine coronene. The C-N distance was between 3.0-3.1 Å and the distance between each oxygen and pyrrolic hydrogen was 2.42 Å. Other similar geometries were obtained, but they are not presented as figures; for example, the NO_2 nitrogen is now the atom that forms the hydrogen bond with the hydrogens of pyrrole, but with lower adsorption energy ($E_{\text{ads}} = 264.90$ meV) than in the previous geometry; the N-H distance were 2.65 and 2.67 Å and nitrogen kept a similar distance from the coronene sheet of 3.0-3.2 Å but this time coordinated with four carbons. A third similar geometry was found. Now, in the bond hydrogen are participating the nitrogen, one of the oxygen atoms of the NO_2 and only one hydrogen of the pyrrole; the distances O...H and N...H were 2.55 and 2.66 Å, respectively, and nitrogen remained at 3.1 Å from coronene with an even lower adsorption energy ($E_{\text{ads}} = 239.88$ meV). The entry of NO_2 molecule with their oxygen atoms pointing to the coronene sheet, made that this molecule rotated itself 90 degrees to acquire the above geometries described. Since various similar geometries converged with very small differences between them, for these configurations, the adsorption energy found was in the range of 240-279 meV.

Table 3. Adsorption energy in meV; $\Delta_{\text{HOMO-LUMO}}$ in eV and Δ ($\Delta_{\text{HOMO-LUMO}}$) values in meV for NO_2 adsorption.

Adsorption complexes	E_{ads}	$\Delta_{\text{HOMO-LUMO}}$	Δ ($\Delta_{\text{HOMO-LUMO}}$)
NH_3 -Coronene	160-176	5.8927	-9.5 *
NH_3 -Coronene-pyrrole (Coronene-free sites)	438-534	5.3438	-343.7 **
NH_3 -Coronene-pyrrole (On pyrrole)	193-208	5.8483	160.8 **

* Obtained in respect of pristine coronene ($\Delta_{\text{HOMO-LUMO}} = 5.9022$ eV).** Obtained in respect of coronene-pyrrole ($\Delta_{\text{HOMO-LUMO}} = 5.6875$ eV).**Figure 6.** HOMO (bottom) and LUMO (top) frontier orbitals of (a) NO_2 -coronene, (b) NO_2 -coronene-pyrrole with NO_2 located over coronene free sites and (c) coronene-pyrrole with NO_2 located over a pyrrole ring.

The NO_2 entry on the pyrrolic ring is presented in Figure 5b; In this geometry, nitrogen is pointing to the pyrrolic ring and two orientations were obtained; In one of them (Figure 5b), nitrogen stayed coordinated with three carbons of the pyrrolic ring with an adsorption energy of 217.14 meV; however, in other similar configuration, nitrogen of NO_2 , positioned itself on the center of the pyrrolic ring in coordination with all the carbons and the nitrogen of this ring, being the adsorption energy of 224.21 meV. In these configurations, the distances between the nitrogen of NO_2 and coronene's carbons were between 3.0-3.2 Å and the distance N-N was 2.99 Å. Finally, in the other configurations, not showed, the interaction between NO_2 and pyrrole did not occur because of the nitrogen of NO_2 but because of the oxygen's atoms; in this geometry, one of the oxygen atoms remained in the center of the pyrrole ring coordinated with the carbon and nitrogen atoms of pyrrole, being the adsorption energy of 181.1 meV.

To sum up, for NO_2 entry, the adsorption energy is kept between 181-279 meV, which is higher than the calculated adsorption energy in pristine coronene molecules (175-207 meV) (Table 2). Furthermore, the highest NO_2 adsorption energy was found on the coronene free sites in the coronene-pyrrole system; this latter result can be related firstly, with the presence of the coronene molecule of activated sites due to the charge transference observed from pyrrole to coronene when both molecules interacted; and secondly, due to the hydrogen bond formed between NO_2 and pyrrole. The magnitude (meV) of the adsorption energy obtained indicates that a physisorption process occurred.

3.5. Coronene-pyrrole- NO_2 system as a NO_2 -sensor

In Table 2, the $\Delta_{\text{HOMO-LUMO}}$ and Δ ($\Delta_{\text{HOMO-LUMO}}$) values included belong to the most favored geometry for the three chosen systems: Coronene- NO_2 , coronene-pyrrole- NO_2 with NO_2 adsorbed on the free sites of coronene sheets and coronene-pyrrole- NO_2 with NO_2 adsorbed on the pyrrole ring. It is important to take into account that if the value of Δ ($\Delta_{\text{HOMO-LUMO}}$) is higher, a more significant change in the electric properties of these systems would be expected as the result of the adsorption processes.

In the three chosen systems, the $\Delta_{\text{HOMO-LUMO}}$ gaps are smaller than the corresponding reference system (without NO_2 adsorbed), indicating a reduction of the gap as a result of the adsorption process; this result led to increase the resistance of the system and it agrees with the experimental tendency of these adsorption systems, in which the adsorbate gas molecule (NO_2) is an electron-acceptor.

In relation to the Δ ($\Delta_{\text{HOMO-LUMO}}$) values, the highest value was obtained for the NO_2 -pyrrole-coronene complex, when NO_2 was adsorbed by the free sites of coronene. It is essential to highlight that, even though a significant change in the gap HOMO-LUMO was observed in the two chosen systems, coronene and pyrrole-coronene, the best candidate would be the latter one because this system showed more favored adsorption sites (coronene free sites). Finally, in Figure 6, the HOMO and LUMO orbital maps are presented; notice the strong π character of both frontier orbitals in the three adsorption systems; however, when NO_2 is located over coronene free sites (Figure 6b), the main contribution of the HOMO orbital comes from pyrrole. On the other hand, the LUMO orbital shows a strong contribution of NO_2 along with coronene orbitals. Even though, the HOMO and LUMO energy levels in NO_2 -pyrrole-coronene decreased respect to the corresponding coronene-pyrrole complex and therefore the orbitals became more binding, the LUMO orbital decreased much more because of the strong overlap between the NO_2 and coronene orbitals (see Figure 6b); therefore, the change in the topology of the frontier orbitals has allowed to explain the significant gap reduction in coronene-pyrrole- NO_2 system, when NO_2 approaches the free sites of coronene.

3.6. Coronene- NH_3 system

The adsorption energy produced by the interaction of NH_3 with pristine coronene was between 160-176 meV (Table 3). Figure 7 shows the optimized geometries for the most probable NH_3 adsorption complexes. The entry of NH_3 with the nitrogen pointing to carbon atoms of the coronene sheet resulted in a N-C distance of 3.11 and 3.30 Å as it can be seen in Figure 7a; in this geometry, with an adsorption energy of 175.5 meV, two hydrogen atoms of NH_3 , are extended over the center of two hexagons, with distances H-C over 2.82-2.85 Å, while the third

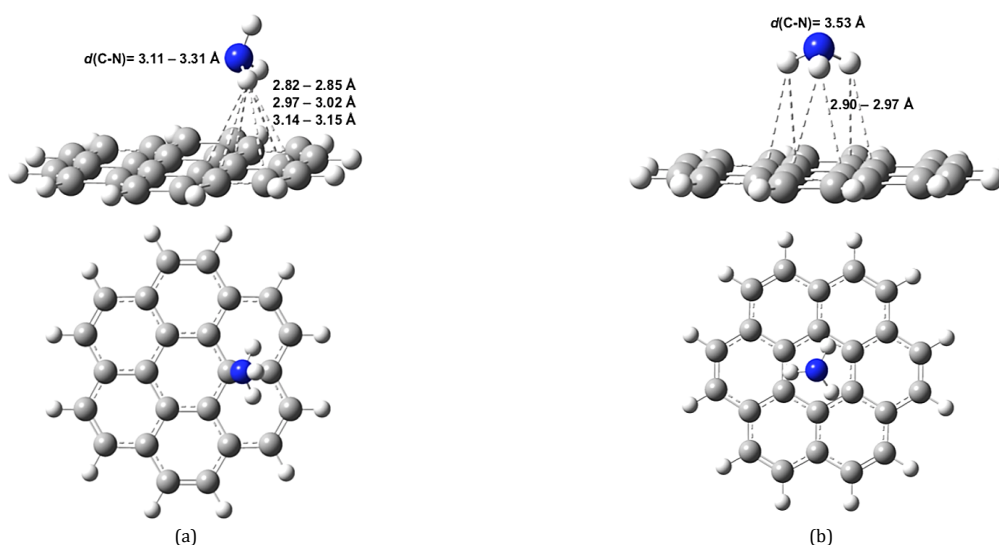


Figure 7. The two most stable optimized geometries for NH_3 adsorption on pristine coronene molecule (a, b).



Figure 8. The most stable optimized geometry for NH_3 adsorption in the coronene-pyrrole system considering NH_3 -entry in the free sites of coronene (a) and over the pyrrole ring (b).

one is oriented upwards. In other favorable orientation, the ammonia was located with its hydrogens pointing to the coronene's central hexagon in a totally symmetrical arrangement where ammonia's hydrogen remained each one on a C-C bond line as [Figure 7b](#) shows; the C-H bond distance kept in the range of 2.92-2.97 Å and the adsorption energy was 169.15 meV. Additionally, other similar geometry was found, in which the hydrogen arrangements were less symmetrical; in this case, the adsorption energy was 160.38 meV.

3.7. Coronene-pyrrole- NH_3 system

In a similar way to NO_2 adsorption, NH_3 was located on the free sites of coronene and over the pyrrole ring. The entry of NH_3 on the free sites of the coronene molecule by both, the ammonia's hydrogen and nitrogen atoms gets similar geometries with adsorption energies of 497.8 and 533.6 meV, respectively ([Table 3](#)), which were much higher than the ones produced by the coronene- NH_3 system; in [Figure 8a](#), the most stable one is presented and you can observe that two hydrogens of the ammonia molecule are coordinated with each of the two carbon atoms of the coronene sheet at a distance of 3.02 and 2.73 Å, while the other hydrogen atom remains oriented upwards. In fact, the most interesting thing is the hydrogen bond formed at 1.90 Å, between the ammonia's nitrogen and the hydrogen which is bonded to the nitrogen of pyrrole. This geometry can be observed in [Figure 8a](#).

The NH_3 entry over pyrrole, throughout its hydrogen atoms produced a unique geometry which is shown in [Figure 8b](#).

Notice that each of the two hydrogen atoms of NH_3 are coordinated with two carbon atoms of the pyrrolic ring at 2.54 and 2.79 Å of distance. Similarly, the nitrogen of the NH_3 molecule is also coordinated with the nitrogen of pyrrole at a distance of 3.14 Å. The adsorption energy for this configuration was 208.0 meV. Finally, another configuration, the one shown in [Figure 8b](#), places the NH_3 -nitrogens on the pyrrole ring center, while one of the NH_3 's hydrogen stays coordinated to the pyrrole-nitrogens at a distance of 3.14 Å; however, for this geometry, the adsorption energy was lower (193.1 meV) ([Table 2](#)). The results of NH_3 adsorption indicated that the adsorption energies in the pyrrole-coronene system are higher (193-534 meV) than those in the pristine coronene system (160-176 meV). Therefore, the functionalization of coronene with pyrrole improves the adsorption process.

3.8. Coronene-pyrrole- NH_3 system as a NH_3 sensor

In [Table 3](#), the $\Delta_{\text{HOMO-LUMO}}$ and Δ ($\Delta_{\text{HOMO-LUMO}}$) of the most representative geometries are presented. Notice that the $\Delta_{\text{HOMO-LUMO}}$ gap of the NH_3 -coronene complex is practically unchanged. However, in the NH_3 -pyrrole-Coronene complexes, two different results are observed; (i) the entrance of NH_3 over the pyrrolic ring which yielded the opening of the HOMO-LUMO gap (Δ ($\Delta_{\text{HOMO-LUMO}}$) = 160.8 meV) according to the electron-acceptor character of NH_3 , which would decrease the conductivity; (ii) the entrance of NH_3 over the free sites of coronene, which yielded the reduction of the HOMO-LUMO gap (Δ ($\Delta_{\text{HOMO-LUMO}}$) = -343.7 meV) contrary to the expected behavior; this could be

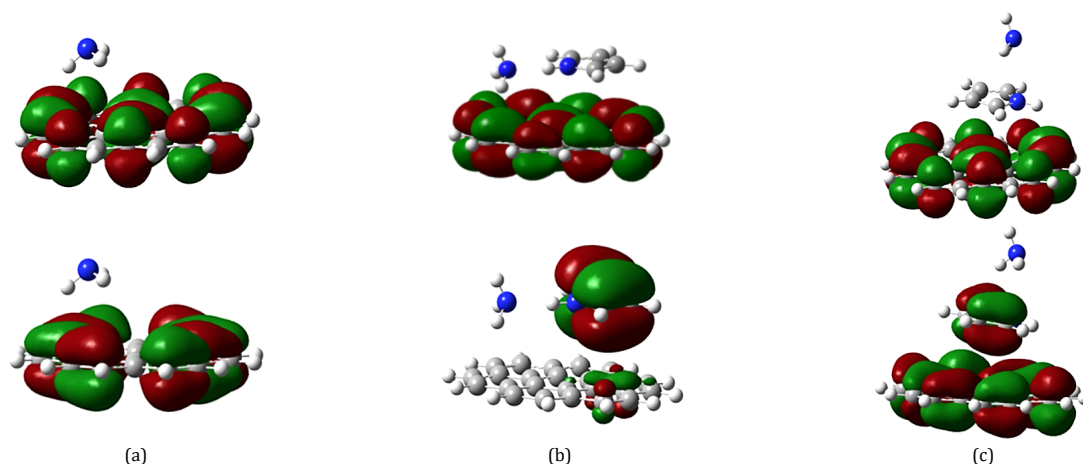


Figure 9. HOMO (bottom) and LUMO (top) frontiers orbitals of (a) NH_3 -coronene, (b) NH_3 -coronene-pyrrole with NH_3 located over coronene free sites and (c) coronene-pyrrole with NH_3 located over pyrrole ring.

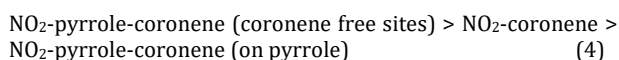
due to the hydrogen bond formed with two of the pyrrole's hydrogens and the position of the NH_3 in the interface pyrrole-coronene; in this case, this adsorption complex might increase the conductivity.

The Δ ($\Delta_{\text{HOMO-LUMO}}$) values indicate that the increase of the conductivity dominates over the decrease. In this way, this system could be recommended as an NH_3 -sensor. These two opposite tendencies observed in Table 3 for the pyrrole-coronene system can be related with two different topology features in the HOMO/LUMO maps presented in Figure 9. When NH_3 is approached over the coronene-free sites (Figure 9b), the contribution of the LUMO orbital comes from coronene essentially and the HOMO orbital contribution comes from pyrrole; however, the contribution of the HOMO orbital, when NH_3 approached over the pyrrole ring (Figure 9c), has to do with the whole coronene-pyrrole complex and for the LUMO orbital only with the coronene part.

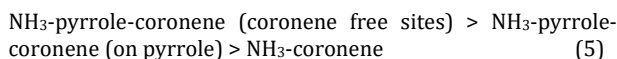
4. Conclusions

The possibilities of using functionalized graphene with pyrrole as a sensor of NO_2 and NH_3 were studied taking into consideration a simple model of a coronene molecule. Previously, the coronene-pyrrole interaction was modelled, and it was found that the pyrrolic ring tended to lie almost parallel to the coronene sheet, in a π - π stacking interaction between the two conjugated systems, being the closest distances about 3.0 and 3.2 Å. To study the adsorption process involving NH_3 and NO_2 molecules, two different sites were considered: on the free sites of coronene, near of the interface coronene-pyrrole, and over the pyrrolic ring. In both adsorption processes, the corresponding energies indicated that the physisorption process had happened; the adsorption energy ranges when the gas molecules were placed on the free sites of coronene resulted higher than in the case in which they were placed over the pyrrolic ring. This result could be related to the formation of a hydrogen bond between the adsorbate molecules and the pyrrolic ring. Moreover, the comparison between the physisorption energies in the pristine coronene system and the coronene-pyrrole system yielded a more favored physisorption process for the latter.

The change in the gap (HOMO-LUMO) in the NO_2 adsorption process presented the following tendency:



Based on the above results, the graphene-pyrrole system could be a better option to be used as a NO_2 -sensor than the pristine graphene one. The change in the gap (HOMO-LUMO) in the NH_3 adsorption process presented the following tendency:



As in the NO_2 -pyrrole-coronene system, when NH_3 is placed on the free sites of coronene, a greater change in the gap was observed; in both cases, as a result of the adsorption process, a reduction of the HOMO-LUMO gap was observed, which could be a descriptor related to the conductivity increase. Although the entry of NH_3 over the pyrrole ring and over the free sites of coronene yielded opposite results (in the former, an opening of the gap was produced, and in the latter a reduction was found), the Δ ($\Delta_{\text{HOMO-LUMO}}$) indicated that the effect of the increase in conductivity was greater than the decreased ones. In this way, this system can also be recommended as a NH_3 -sensor. Notice that in the NH_3 -coronene (pristine), the magnitude of the change was non-significant; accordingly, we consider it is not appropriate nor advisable to use it as a NH_3 -sensor. These results allowed us to conclude that Δ ($\Delta_{\text{HOMO-LUMO}}$) can be an easy and suitable descriptor for characterizing the performance of a sensor.

Acknowledgements

We gratefully acknowledge the generous computing time provided by Dirección General de Cómputo y de Tecnologías de Información y Comunicación at the Universidad Nacional Autónoma de México (DGTIC-UNAM) through the Grants LANCAD-UNAM-DGTIC-156. This research was supported by a grant from the "Cátedra de Investigación CI2202"-FES-Cuautitlán-UNAM and COMECyT project FICDTEM-2021-080.

Disclosure statement

Conflict of interest: The authors declare that they have no conflict of interest. Ethical approval: All ethical guidelines have been adhered.

CRedit authorship contribution statement

Conceptualization: Esther Agacino-Valdés; Methodology: Esther Agacino-Valdés, Cinthya Susana Olmedo-Martínez, Sandy María Pacheco-Ortín, Roberto Mejía-Olvera; Software: J. Moisés Hernández-Duarte, Cinthya Susana Olmedo-Martínez; Validation: Cinthya Susana Olmedo-Martínez; Formal Analysis: Esther Agacino-Valdés, Roberto Mejía-Olvera, Sandy María Pacheco-Ortín; Investigation: Esther Agacino-Valdés, Cinthya Susana Olmedo-Martínez, Roberto Mejía-Olvera, Sandy María Pacheco-Ortín, J. Moisés Hernández-Duarte; Resources: Esther Agacino-Valdés; Writing - Original Draft: Esther Agacino-Valdés; Writing - Review and Editing: Esther

Agacino-Valdés, Cinthya Susana Olmedo-Martínez, Roberto Mejía-Olvera, Sandy María Pacheco-Ortín; Visualization: Cinthya Susana Olmedo-Martínez, J. Moisés Hernández-Duarte; Supervision: Esther Agacino-Valdés; Project Administration: Esther Agacino Valdés.

ORCID and Email

Cinthya Susana Olmedo-Martínez

 cinthya-olm@cuautitlan.unam.mx

 <https://orcid.org/0000-0002-2833-6062>

Jesús Moisés Hernández-Duarte

 hduarte@unam.mx

 <https://orcid.org/0000-0003-1724-3765>

Roberto Mejía-Olvera

 roberto.mo@cuautitlan.tecnm.mx

 <https://orcid.org/0000-0003-2895-815X>

Sandy-María Pacheco-Ortín

 sm pocquimicas@comunidad.unam.mx

 <https://orcid.org/0000-0003-2477-1101>

Esther Agacino-Valdés

 eagacino@unam.mx

 <https://orcid.org/0000-0002-5386-8933>

References

- Novoselov, K. S.; Geim, A. K.; Morozov, S. V.; Jiang, D.; Zhang, Y.; Dubonos, S. V.; Grigorieva, I. V.; Firsov, A. A. Electric field effect in atomically thin carbon films. *Science* **2004**, *306*, 666–669.
- Lee, C.; Wei, X.; Kysar, J. W.; Hone, J. Measurement of the elastic properties and intrinsic strength of monolayer graphene. *Science* **2008**, *321*, 385–388.
- Castro Neto, A. H.; Guinea, F.; Peres, N. M. R.; Novoselov, K. S.; Geim, A. K. The electronic properties of graphene. *Rev. Mod. Phys.* **2009**, *81*, 109–162.
- Morozov, S. V.; Novoselov, K. S.; Katsnelson, M. I.; Schedin, F.; Elias, D. C.; Jaszczak, J. A.; Geim, A. K. Giant intrinsic carrier mobilities in graphene and its bilayer. *Phys. Rev. Lett.* **2008**, *100*, 016602.
- Allen, M. J.; Tung, V. C.; Kaner, R. B. Honeycomb carbon: a review of graphene. *Chem. Rev.* **2010**, *110*, 132–145.
- Schedin, F.; Geim, A. K.; Morozov, S. V.; Hill, E. W.; Blake, P.; Katsnelson, M. I.; Novoselov, K. S. Detection of individual gas molecules adsorbed on graphene. *Nat. Mater.* **2007**, *6*, 652–655.
- Yavari, F.; Koratkar, N. Graphene-based chemical sensors. *J. Phys. Chem. Lett.* **2012**, *3*, 1746–1753.
- Kochmann, S.; Hirscht, T.; Wolfbeis, O. S. Graphenes in chemical sensors and biosensors. *Trends Analyt. Chem.* **2012**, *39*, 87–113.
- Varghese, S. S.; Lonkar, S.; Singh, K. K.; Swaminathan, S.; Abdala, A. Recent advances in graphene based gas sensors. *Sens. Actuators B Chem.* **2015**, *218*, 160–183.
- Wang, T.; Huang, D.; Yang, Z.; Xu, S.; He, G.; Li, X.; Hu, N.; Yin, G.; He, D.; Zhang, L. A review on graphene-based gas/vapor sensors with unique properties and potential applications. *Nanomicro Lett.* **2016**, *8*, 95–119.
- Abdelhalim, A. O. E.; Semenov, K. N.; Nerukh, D. A.; Murin, I. V.; Maistrenko, D. N.; Molchanov, O. E.; Sharoyko, V. V. Functionalisation of graphene as a tool for developing nanomaterials with predefined properties. *J. Mol. Liq.* **2022**, *348*, 118368.
- Qian, Z.; Ma, J.; Shan, X.; Shao, L.; Zhou, J.; Chen, J.; Feng, H. Surface functionalization of graphene quantum dots with small organic molecules from photoluminescence modulation to bioimaging applications: an experimental and theoretical investigation. *RSC Adv.* **2013**, *3*, 14571.
- Yu, L.; Gao, H.; Zhao, J.; Qiu, J.; Yu, C. Adsorption of aromatic heterocyclic compounds on pristine and defect graphene: A first-principles study. *J. Comput. Theor. Nanosci.* **2011**, *8*, 2492–2497.
- Zhang, Y.-H.; Chen, Y.-B.; Zhou, K.-G.; Liu, C.-H.; Zeng, J.; Zhang, H.-L.; Peng, Y. Improving gas sensing properties of graphene by introducing dopants and defects: a first-principles study. *Nanotechnology* **2009**, *20*, 185504.
- Boukhvalov, D. W.; Katsnelson, M. I. Chemical functionalization of graphene. *J. Phys. Condens. Matter* **2009**, *21*, 344205.
- Alzate-Carvajal, N.; Luican-Mayer, A. Functionalized graphene surfaces for selective gas sensing. *ACS Omega* **2020**, *5*, 21320–21329.
- Tang, X.; Debliquy, M.; Lahem, D.; Yan, Y.; Raskin, J.-P. A review on functionalized graphene sensors for detection of ammonia. *Sensors (Basel)* **2021**, *21*, 1443.
- Adhikari, B.; Majumdar, S. Polymers in sensor applications. *Prog. Polym. Sci.* **2004**, *29*, 699–766.
- Panapimonlawat, T.; Phanichphant, S.; Sriwichai, S. Electrochemical dopamine biosensor based on poly(3-aminobenzylamine) layer-by-layer self-assembled multilayer thin film. *Polymers (Basel)* **2021**, *13*, 1488.
- Sadek, A. Z.; Wlodarski, W.; Kalantar-Zadeh, K.; Baker, C.; Kaner, R. B. Doped and dedoped polyaniline nanofiber based conductometric hydrogen gas sensors. *Sens. Actuators A Phys.* **2007**, *139*, 53–57.
- Virji, S.; Kaner, R. B.; Weiller, B. H. Hydrogen sensors based on conductivity changes in polyaniline nanofibers. *J. Phys. Chem. B* **2006**, *110*, 22266–22270.
- Al-Mashat, L.; Shin, K.; Kalantar-zadeh, K.; Plessis, J. D.; Han, S. H.; Kojima, R. W.; Kaner, R. B.; Li, D.; Gou, X.; Ippolito, S. J.; Wlodarski, W. Graphene/polyaniline nanocomposite for hydrogen sensing. *J. Phys. Chem. C Nanomater. Interfaces* **2010**, *114*, 16168–16173.
- Liu, X.; Ly, J.; Han, S.; Zhang, D.; Requiha, A.; Thompson, M. E.; Zhou, C. Synthesis and electronic properties of individual single-walled carbon nanotube/polypyrrole composite nanocables. *Adv. Mater.* **2005**, *17*, 2727–2732.
- Leenaerts, O.; Partoens, B.; Peeters, F. M. Adsorption of H₂O, NH₃, CO, NO₂, and NO on graphene: A first-principles study. *Phys. Rev. B Condens. Matter Mater. Phys.* **2008**, *77*, 125416.
- Bonfanti, M.; Martinazzo, R.; Tantardini, G. F.; Ponti, A. Physisorption and Diffusion of Hydrogen Atoms on Graphite from Correlated Calculations on the H-Coronene Model System. *J. Phys. Chem. C* **2007**, *111*, 16, 5825–5829.
- Mattson, E. C.; Pande, K.; Unger, M.; Cui, S.; Lu, G.; Gajdardziska-Josifovska, M.; Weinert, M.; Chen, J.; Hirschmugl, C. J. Exploring adsorption and reactivity of NH₃ on reduced graphene oxide. *J. Phys. Chem. C Nanomater. Interfaces* **2013**, *117*, 10698–10707.
- Jang, W.-K.; Yun, J.; Kim, H.-I.; Lee, Y.-S. Improvement of ammonia sensing properties of polypyrrole by nanocomposite with graphitic materials. *Colloid Polym. Sci.* **2013**, *291*, 1095–1103.
- Frisch, M. J.; Trucks, G. W.; Schlegel, H. B.; Scuseria, G. E.; Robb, M. A.; Cheeseman, J. R.; Montgomery, J. A.; Vreven, T.; Kudin, K. N.; Burant, J. C.; Millam, J. M.; Iyengar, S. S.; Tomasi, J.; Barone, V.; Mennucci, B.; Cossi, M.; Scalmani, G.; Rega, N.; Petersson, G. A.; Nakatsuji, H.; Hada, M.; Ehara, M.; Toyota, K.; Fukuda, R.; Hasegawa, J.; Ishida, M.; Nakajima, T.; Honda, Y.; Kitao, O.; Nakai, H.; Klene, M.; Li, X.; Knox, J. E.; Hratchian, H. P.; Cross, J. B.; Adamo, C.; Jaramillo, J.; Gomperts, R.; Stratmann, R. E.; Yazyev, O.; Austin, A. J.; Cammi, R.; Pomelli, C.; Ochterski, J. W.; Ayala, P. Y.; Morokuma, K.; Voth, G. A.; Salvador, P.; Dannenberg, J. J.; Zakrzewski, V. G.; Dapprich, S.; Daniels, A. D.; Strain, M. C.; Farkas, O.; Malick, D. K.; Rabuck, A. D.; Raghavachari, K.; Foresman, J. B.; Ortiz, J. V.; Cui, Q.; Baboul, A. G.; Clifford, S.; Cioslowski, J.; Stefanov, B. B.; Liu, G.; Liashenko, A.; Piskorz, P.; Komaromi, I.; Martin, R. L.; Fox, D. J.; Keith, T.; Al-Laham, M. A.; Peng, C. Y.; Nanayakkara, A.; Challacombe, M.; Gill, P. M. W.; Johnson, B.; Chen, W.; Wong, M. W.; Gonzalez, C.; Pople, J. A. Gaussian, Inc., Wallingford CT, 2009.
- Zhao, Y.; Truhlar, D. G. The M06 suite of density functionals for main group thermochemistry, thermochemical kinetics, noncovalent interactions, excited states, and transition elements: two new functionals and systematic testing of four M06-class functionals and 12 other functionals. *Theor. Chem. Acc.* **2008**, *120*, 215–241.
- Hohenstein, E. G.; Chill, S. T.; Sherrill, C. D. Assessment of the Performance of the M05–2X and M06–2X Exchange-Correlation Functionals for Noncovalent Interactions in Biomolecules. *J. Chem. Theory Comput.* **2008**, *4*, 12, 1996–2000.
- Rohini, K.; Sylvinson, D. M. R.; Swathi, R. S. Intercalation of HF, H₂O, and NH₃ clusters within the bilayers of graphene and graphene oxide: Predictions from coronene-based model systems. *J. Phys. Chem. A* **2015**, *119*, 10935–10945.
- Yeamin, M. B.; Faginas-Lago, N.; Albertí, M.; Cuesta, I. G.; Sánchez-Marín, J.; Sánchez de Merás, A. M. J. Multi-scale theoretical investigation of molecular hydrogen adsorption over graphene: coronene as a case study. *RSC Adv.* **2014**, *4*, 54447–54453.
- Wilson, J.; Faginas-Lago, N.; Vekeman, J.; Cuesta, I. G.; Sánchez-Marín, J.; Sánchez de Merás, A. Modeling the interaction of carbon monoxide with flexible graphene: From coupled cluster calculations to molecular-dynamics simulations. *Chemphyschem* **2018**, *19*, 774–783.
- Petrushenko, I. K.; Petruschenko, K. B. Physical adsorption of N-containing heterocycles on graphene-like boron nitride-carbon heterostructures: A DFT study. *Comput. Theor. Chem.* **2017**, *1117*, 162–168.
- Rad, A. S.; Shabestari, S. S.; Mohseni, S.; Aghouzi, S. A. Study on the adsorption properties of O₃, SO₂, and SO₃ on B-doped graphene using DFT calculations. *J. Solid State Chem.* **2016**, *237*, 204–210.
- Wanno, B.; Tabtimsai, C. A DFT investigation of CO adsorption on VIIIb transition metal-doped graphene sheets. *Superlattices Microstruct.* **2014**, *67*, 110–117.
- Anota, E. C.; Villanueva, M. S.; Cocoltzi, H. H. Density functional theory study of lithium and fluoride doped boron nitride sheet. *Phys. Status Solidi C* **2010**, *7*, 2559–2561.

- [38]. Velázquez-López, L.-F.; Pacheco-Ortín, S.-M.; Mejía-Olvera, R.; Agacino-Valdés, E. DFT study of CO adsorption on nitrogen/boron doped-graphene for sensor applications. *J. Mol. Model.* **2019**, *25*, 91.
- [39]. Chung, L. W.; Sameera, W. M. C.; Ramozzi, R.; Page, A. J.; Hatanaka, M.; Petrova, G. P.; Harris, T. V.; Li, X.; Ke, Z.; Liu, F.; Li, H.-B.; Ding, L.; Morokuma, K. The ONIOM method and its applications. *Chem. Rev.* **2015**, *115*, 5678–5796.
- [40]. Mayhall, N. J.; Raghavachari, K. Molecules-in-molecules: An extrapolated fragment-based approach for accurate calculations on large molecules and materials. *J. Chem. Theory Comput.* **2011**, *7*, 1336–1343.
- [41]. Zhang, Z.; Huang, H.; Yang, X.; Zang, L. Tailoring electronic properties of graphene by π - π stacking with aromatic molecules. *J. Phys. Chem. Lett.* **2011**, *2*, 22, 2897–2905.



Copyright © 2022 by Authors. This work is published and licensed by Atlanta Publishing House LLC, Atlanta, GA, USA. The full terms of this license are available at <http://www.eurjchem.com/index.php/eurjchem/pages/view/terms> and incorporate the Creative Commons Attribution-Non Commercial (CC BY NC) (International, v4.0) License (<http://creativecommons.org/licenses/by-nc/4.0>). By accessing the work, you hereby accept the Terms. This is an open access article distributed under the terms and conditions of the CC BY NC License, which permits unrestricted non-commercial use, distribution, and reproduction in any medium, provided the original work is properly cited without any further permission from Atlanta Publishing House LLC (European Journal of Chemistry). No use, distribution or reproduction is permitted which does not comply with these terms. Permissions for commercial use of this work beyond the scope of the License (<http://www.eurjchem.com/index.php/eurjchem/pages/view/terms>) are administered by Atlanta Publishing House LLC (European Journal of Chemistry).